International Journal of Automotive Technology, Vol. 8, No. 4, pp. 455–465 (2007)

1229–9138/2007/035–08

EXPERIMENTAL STUDY ON THE BUSHING CHARACTERISTICS UNDER SEVERAL EXCITATION INPUTS FOR BUSHING MODELING

J. K. OK[1)], W. S. YOO[1)] and J. H. SOHN[2)*]

[1)]School of Mechanical Engineering, Pusan National University, Busan 609-735, Korea
[2)]School of Mechanical Engineering, Pukyong National University, Busan 608-739, Korea

(Received 5 February 2007; Revised 11 June 2007)

ABSTRACT–The bushing element shows nonlinear characteristics in both displacements and frequencies, also with hysteretic responses for repeated vibrational excitations. Since the characteristics of the rubber bushing significantly affects the accuracy of the vehicle dynamic simulation result, it should be accurately modeled in the vehicle suspension model. To develop an accurate bushing model for vehicle dynamics analysis, the bushing characteristics under several excitation inputs must be known. In this paper, a 3-axis tester was used to capture the bushing characteristics. The random inputs, sine inputs, and step inputs were imposed on each axis of the bushing. Also, two-axis inputs, the radial-axial and radial-normal inputs, were simultaneously imposed on the tester. Three-axis inputs including the radial-axial-normal direction were supplied to the tester. Bushing characteristics of each case were precisely analyzed. These results could be available for dynamic modeling of bushing.

KEY WORDS : Bushing model, Rubber tester, Hysteresis, Vehicle dynamic analysis

NOMENCLATURE

δ_i : bushing excitation displacement
$\delta_{a,i}$: bushing displacement of axial direction
$\delta_{n,i}$: bushing displacement of normal direction
$\delta_{r,i}$: bushing displacement of radial direction
f : exitation frequency
T_j^* : rise time of step input
n : index of random profile

1. INTRODUCTION

The bushing element is a hollow cylinder connecting the outer steel cylindrical sleeve and the inner steel cylindrical rod. The inner rod is connected to the vehicle chassis and is used to transfer forces from the wheel to the chassis. Due to the rubber material in the bushing, it has nonlinear characteristics for both displacements and frequencies along with hysteretic responses for repeated vibration excitations. Since the characteristics of the rubber bushing significantly affects the accuracy of the vehicle dynamic simulation results, it should be taken into account in the vehicle suspension model (Choi *et al.*, 2005; ADAMS, 2003; RecurDyn, 2005). The bushing forces depend not only on instantaneous deformation but also on the history of deformation. As a result, the hysteretic restoring force cannot be expressed by an algebraic function of the instantaneous displacement and velocity. These history-dependent characteristics of a bushing renders the hysteretic systems more difficult to model and analyze than other non-linear systems (Sohn *et al.*, 2007). There are many approaches in modeling the bushing element for vehicle dynamic simulations (Barber, 2000; Ok *et al.*, 2006). Lee and Wineman (2000) presented a 2-axis model including axial and torsional displacement. Dzierzek (2000) carried out radial-normal coupled mode simulations by making the inclination angle from the radial direction against the normal direction to be 30° and 60°. However, these cases do not consider the 3-axis model of the real vehicle system. It is necessary to accurately capture the bushing characteristics to make these kinds of bushing models. Kuo (1997) carried out some tests for bushing. However, two axes- and three axes-coupled tests have not been performed. To make an accurate bushing model for vehicle dynamics analysis, the bushing characteristics under several excitation inputs must be known.

In this paper, a 3-axis MTS rubber tester is used to capture the bushing characteristics. 1-axis, 2-axis, and 3-axis test are carried out, respectively. Initially, 1-axis tests about the radial and the axial directions are performed. Since the normal direction is the same as the radial

*Corresponding author. e-mail: jhsohn@pknu.ac.kr

direction, the 1-axis test about the normal direction is skipped. The sine inputs are imposed on each axis to investigate the characteristics due to the displacement and frequency. The step inputs according to the delay time are applied to the bushing and capture the steady state characteristics. In addition, the random inputs are imposed on each axis. Next, the coupled excitations about the radial-axial and radial-normal direction are applied to the bushing according to the sine and step inputs. For the radial-axial coupled tests, the axial direction excitations are changed and investigated with the fixed radial input. Also, the radial direction excitations are changed and investigated with the fixed axial input. Finally, 3-axis tests about the radial-normal-axial coupled direction are carried out according to the sine and step inputs. The characteristics from the 3-axis tests are compared with the 1-axis and 2-axis tests. These results could be applied to develop a precise bushing modeling for vehicle dynamic simulations.

Experimental setup and radial and axial direction tests results were shown and explained in chapter 2. The coupled mode tests such as 2-axis and 3-axis results were shown in chapter 3. Some conclusions from the experimental results were described in chapter 4.

2. RADIAL AND AXIAL TESTS

Bushing coordinate systems as shown in Figure 1 are used in this study (SAE, 2000). The 3-axis elastomer testing system and the configuration of the bushing characteristics are shown in Figures 2 and 3, respectively. Specifications for the MTS 3-axis rubber tester and bushing are shown in the Table 1 and 2, respectively. A constant temperature chamber was used to remove the effect of temperature and bushing tests were carried out at a 25°C operating temperature.

2.1. One-axis Harmonic Test

2.1.1. Harmonic test specifications

The purpose of harmonic tests are to determine bushing stiffness and damping characteristics as a function of displacement and frequency. The harmonic tests were conducted for several different frequencies and displacements shown in Table 3. Displacement inputs were set to have limits of 10,000 N in the radial direction and 2,000N

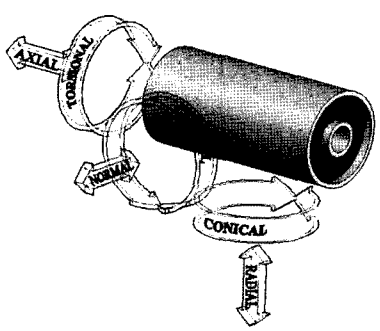

Figure 1. Bushing coordinate systems.

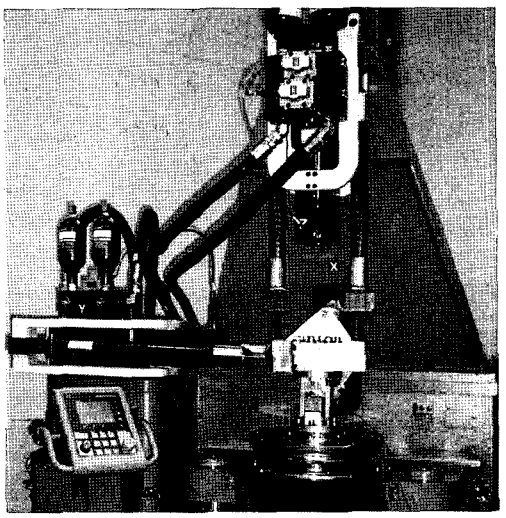

Figure 2. Three-axis elastomer testing system.

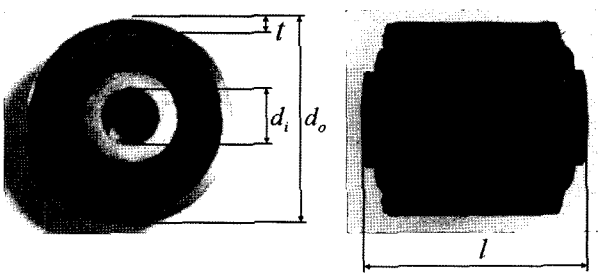

Figure 3. Bushing configuration.

Table 1. Specifications of the bushing tester.

Item	3-axis Elastomer Testing System
Maximum dynamic force	25.0 [kN]
Maximum static force	37.5 [kN]
Maximum dynamic length	25.0 [mm]
Frequency	0.1~80.0 [Hz]
Data acquisition rate	over 6.0 [kHz]

Table 2. Specifications of the test bushing.

Item	Magnitude
Outer steel diameter (d_o)	50 [mm]
Inner steel diameter (d_i)	15 [mm]
Length (l)	63 [mm]
Outer steel thickness (t)	3 [mm]

Table 3. Frequency and displacement in harmonic inputs.

Item	Radial	Axial
Frequency f [Hz]	1, 10, 20, 30	1, 10, 20, 30
Displacement δ_i [mm]	0.5, 1.0, 2.0, 3.0	1.0, 2.0, 3.0, 4.0

in the axial direction, respectively. In the tests, the radial displacement limit was set to 3.0 mm and the axial displacement limit was 4.0 mm.

The excitation according to time can be represented as;

$$\delta(t) = \delta_i \sin 2\pi f t \quad (1)$$

Since the power spectral density of a bushing load measured on a rough road for durability analysis at a proving ground typically exhibited a peak value in the range of 10~15 Hz, the maximum frequency for the test was assigned a value of 30 Hz. The forces of the rubber bush due to change of the displacement and the frequency were measured for 60 seconds.

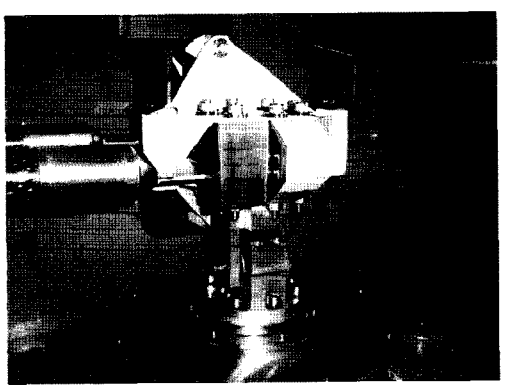

Figure 4. Test jig for bushing experiment.

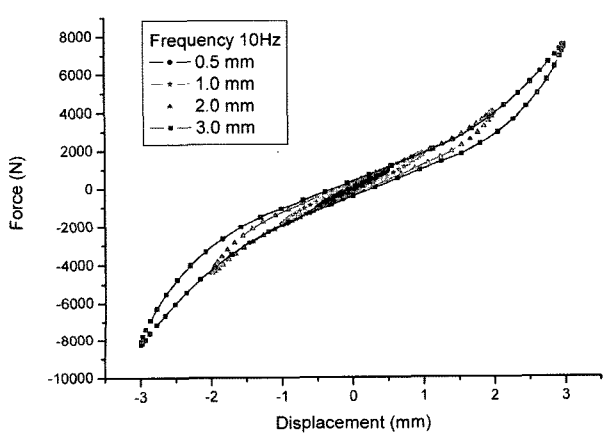

Figure 5. Radial forces according to the displacement.

2.1.2. Radial harmonic test

The test jig is as shown in Figure 4. Radial bushing forces according to the displacement at a 10 Hz excitation input is shown in Figure 5 and radial bushing forces with respect to the frequency at a 3.0 mm excitation is represented in Figure 6. As shown in Figure 5, the characteristics of the bushing force tend to be more nonlinear according to the displacement increase. As the bushing displacement exceeds 1.0 mm, the nonlinear tendency of the bushing force is increased. The slope of the bushing is constant in the linear region but the bushing slopes become more steep due to the frequency increase as shown in Figure 6.

2.1.3. Axial harmonic test

Axial bushing forces according to displacement with an 10 Hz excitation input is shown in Figure 7 and axial bushing forces according to the frequency with 4.0 mm excitation is represented in Figure 8. As shown in Figure 7, the characteristics of the bushing force show a linear

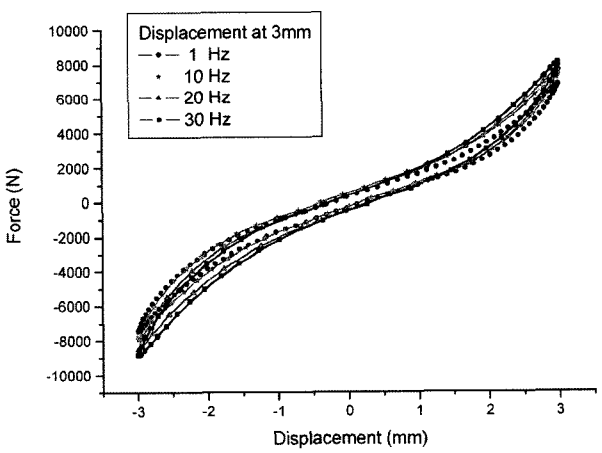

Figure 6. Radial forces according to the frequency.

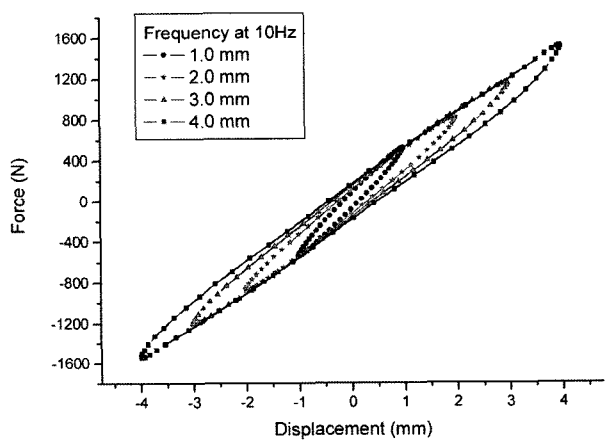

Figure 7. Axial forces according to the displacement.

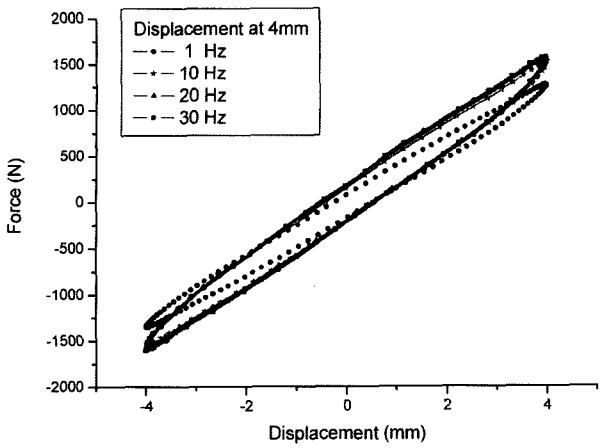

Figure 8. Axial forces according to the frequency.

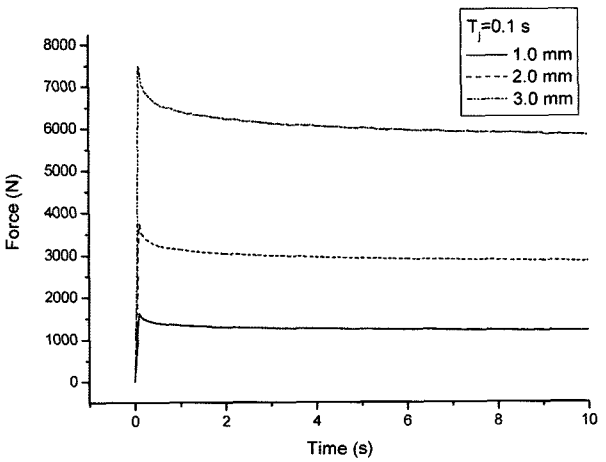

Figure 9. Radial forces according to the displacement.

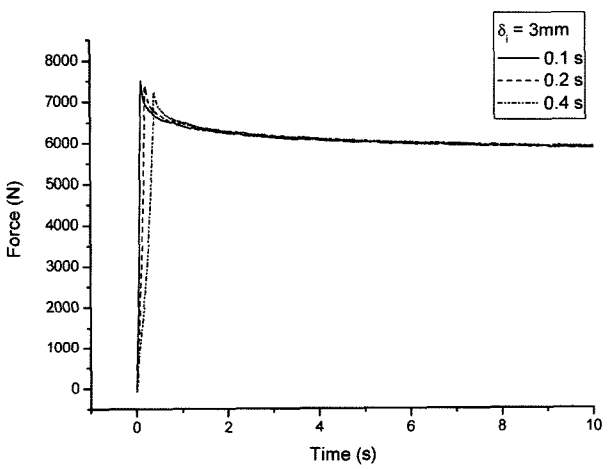

Figure 10. Radial forces according to the time delay.

tendency as displacement increases. In the Figure 8, when the frequency comes over 10 Hz, the slope is changed and kept the same value according to change the frequency.

2.2. One-axis Step Input Test

2.2.1. Step input test specifications

Bushings under the step input show the relaxation characteristics. Tests are carried out with several different displacements and rise times as shown in Table 4. When the time reaches the rise time T_j^*, the excitation input written equation (2) is applied proportionally. After the rise time, the displacement is kept at δ_i.

$$\delta(t) = \frac{\delta_i}{T_j^*} t, \quad 0 \le t \le T_j^* \qquad (2)$$
$$= \delta_i, \quad T_j^* \le t \le 10s$$

2.2.2. Radial step input test

Radial bushing forces with respect to the displacement in the case of 0.1 second rise time are shown in Figure 9 and radial bushing forces with respect to the rise time under a 3.0 mm excitation input is represented in Figure 10.

As shown in the Figure 9, when the rise time is 0.1 s, radial bushing forces are 7510 N, 3740 N, 1620 N, respectively. Figure 10 shows the radial bushing forces with respect to the rise time under the displacement 3.0 mm. In Figure 10, as the rise time decreases, the bushing forces increase. Therefore, the results of Figure 9 are verified within a 5% error range. When the step input is imposed and displacement is kept constant, the bushing forces decrease slowly and reach steady state (value in 5% of final value) in 2.8 s regardless of the magnitude of the displacement input.

Table 4. Displacements and rise times of step inputs.

Item	Radial	Axial
Displacements δ_i [mm]	1.0, 2.0, 3.0	2.0, 3.0, 4.0
Rise time T_j^* [second]	0.1, 0.2, 0.4	0.1, 0.2, 0.4

2.2.3. Axial step input test

Axial bushing forces according to the displacement in the case of a 0.1 s rise time is shown in Figure 11 and axial bushing forces with respect to the rise time under a 4.0 mm excitation input is represented in Figure 12.. As shown in Figures 11 and Figure 12, the characteristics of axial bushing force show a linear tendency with respect to the rise time.

2.3. One-axis Random Input Test

2.3.1. Random input test specifications

The random input data were generated by using RPC PRO software supported by MTS, Inc. The RPC PRO software has the following sampling rates, i.e., 51.2, 64,

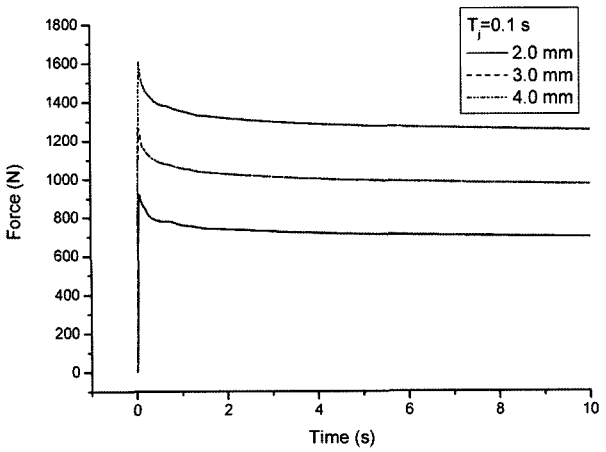

Figure 11. Axial forces according to the displacement.

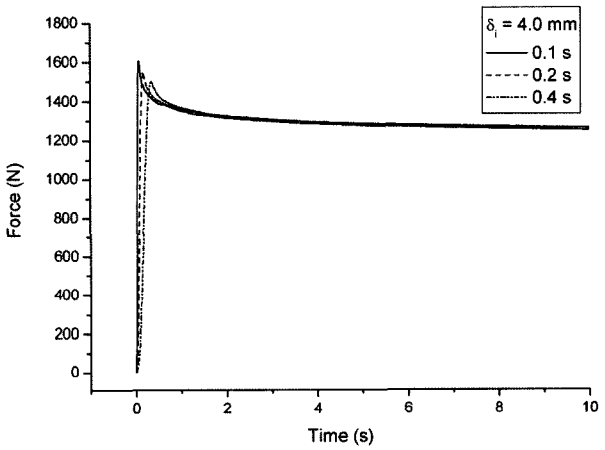

Figure 12. Axial forces according to the rise time.

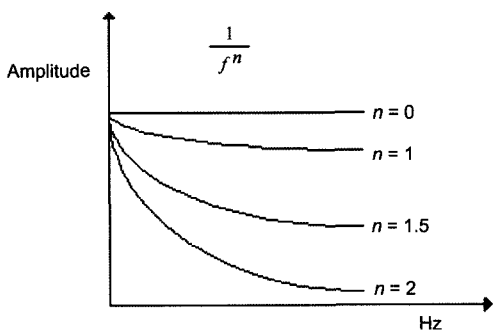

Figure 13. Displacement of random data due to the change of index 'n'.

102.4, 204.8, 256, 409.6, 512, 1024, 2048 Hz. Since a sampling rate of 1024 Hz was chosen with a frame size of 8192 points per frame, the time interval was calculated as 9.765625e-4. Figure 13 shows the displacement of random data in frequency domain due to the change in index 'n'.

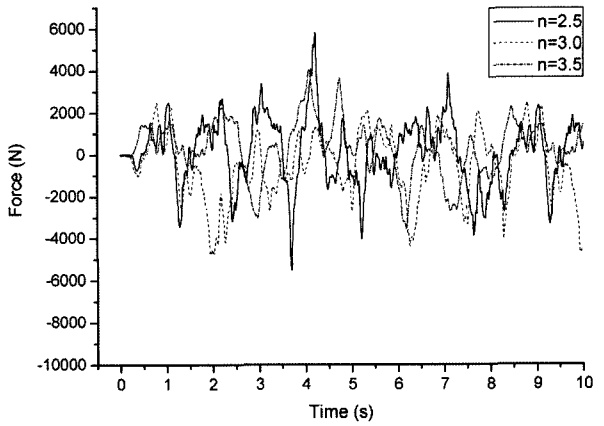

Figure 14. Radial forces under random excitation.

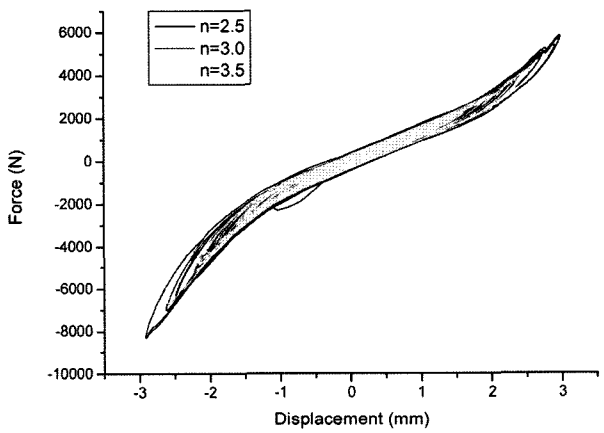

Figure 15. Displacement vs radial forces under random excitation.

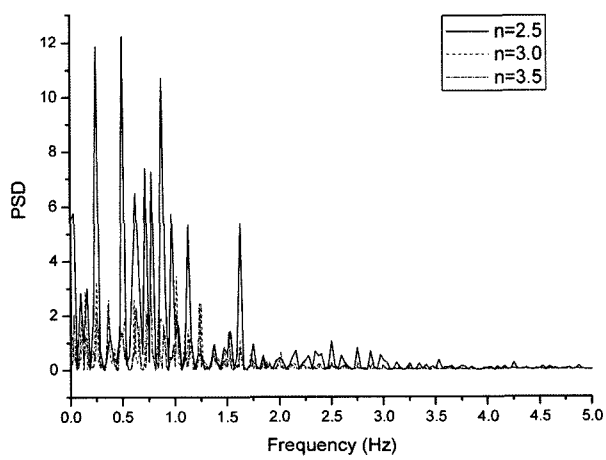

Figure 16. PSD of radial forces.

An index 'n' of 2.5, 3.0, 3.5 is used in this study.

2.3.2. Radial random input test

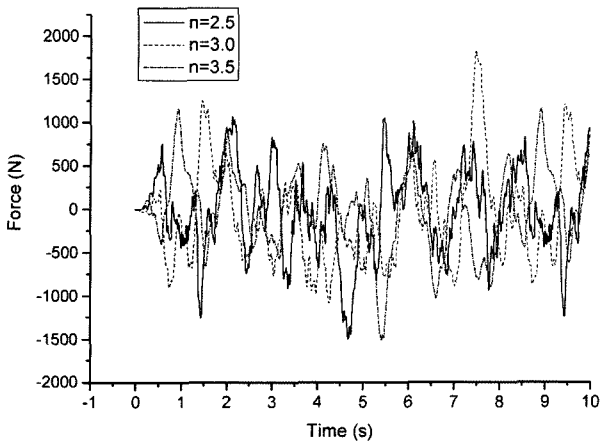

Figure 17. Axial forces under random excitation inputs.

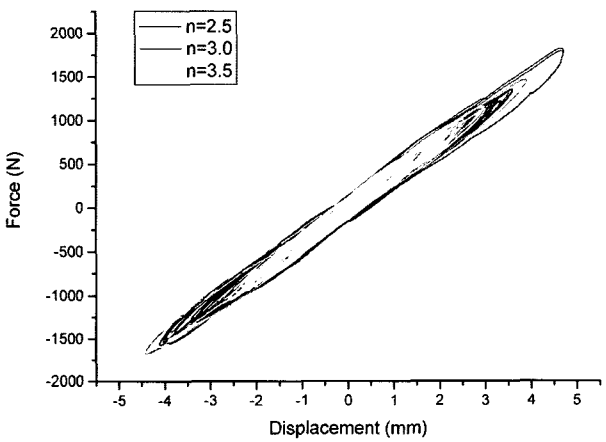

Figure 18. Displacement vs axial forces under random excitation inputs.

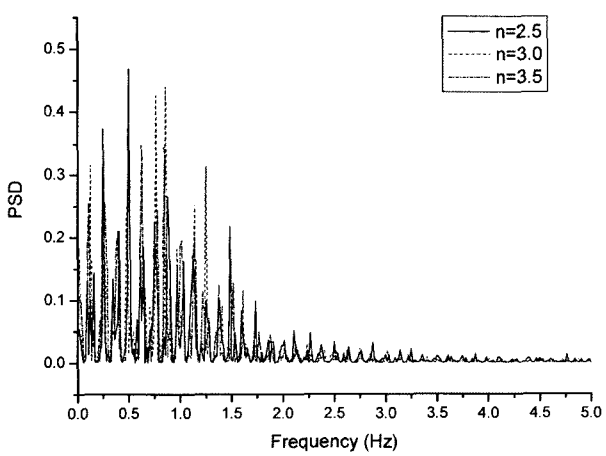

Figure 19. PSD of axial forces.

Radial bushing forces under random excitation inputs are shown in Figure 14 and displacement-force relationships are shown in Figure 15. Since excitation time needs to be more than 60 seconds to make the excitation frequency range be 30 Hz, it is set to 65 seconds in this study. As shown in Figure 13, the bigger the 'n' value is, the smaller the displacement input becomes. As shown in the Figure 16, the bigger the 'n' value is, the smaller PSD becomes.

Table 5. Specifications of coupled tests (radial+axial).

Item	Radial (mm)	Axial (mm)
Displacements (δ_i)	1.0, 2.0, 3.0	1.0, 2.0, 3.0, 4.0

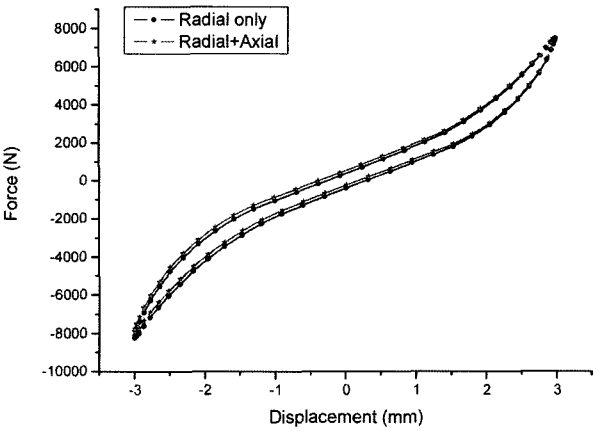

Figure 20. Comparison of radial forces (radial only versus radial-axial coupled).

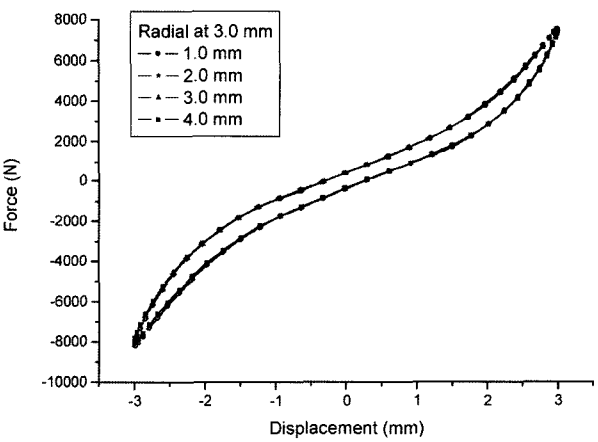

Figure 21. Radial bushing forces according to the different axial input ($\delta_{a,i}$ = 1.0, 2.0, 3.0, 4.0 mm).

2.3.3. Axial random input test

Axial bushing forces under random excitation inputs are shown in Figure 17 and displacement-force relationships are shown in Figure 18. The axial bushing forces due to the random input show linear characteristics. As shown in the Figure 19, the PSD seldom appears in the region

over 5 Hz.

3. COUPLED MODE TESTS

3.1. Coupled Test of Radial and Axial

3.1.1. Two-axis test under sine wave excitation

In the real vehicle system, multi-axial forces are frequently applied to the bushing. To consider these cases, 12 types of coupled testing as shown in Table 5 are carried out.

Figure 20 compares the radial force with a 3.0 mm radial input to a combined force in 3.0 mm rdial and 4.0 mm axial inputs. As shown in Figure 20, the error between two cases is within 5% and can be neglibible since it may be caused by the sensor and the repeated test. Figure 21 presents the radial bushing forces with a 3.0 mm radial input according to 1.0, 2.0, 3.0, and 4.0 mm axial inputs. Even though the axial inputs are changed, the radial bushing forces are not affected by them. This is because the bushing used in this study is designed to have mainly radial forces and the radial stiffness is about 5 times larger than the axial stiffness.

Figure 22 compares the axial bushing forces with a 4.0 mm axial input only to a coupled input of 4.0 mm in the axial and 3.0 mm in the radial direction. Compared to the axial direction only, the coupled result shows nonlinear characteristics. Figure 23 presents the axial bushing forces with a 4.0 mm axial input according to 1.0, 2.0, and 3.0 mm radial inputs. Whenever the radial input is increased, the nonlinear characteristics are bigger.

3.1.2. Two-axis test with step input excitation

Figure 24 shows the radial bushing forces with a 4.0 mm axial input according to several step input excitations. Table 6 presents differencies of maximum radial bushing forces due to the coupled step input with a 4.0 mm axial input. The maximum force is less than 1.56% and has little effect on the axial input.

Figure 25 shows the axial bushing forces with a 3.0 mm radial input according to several step input excitations.

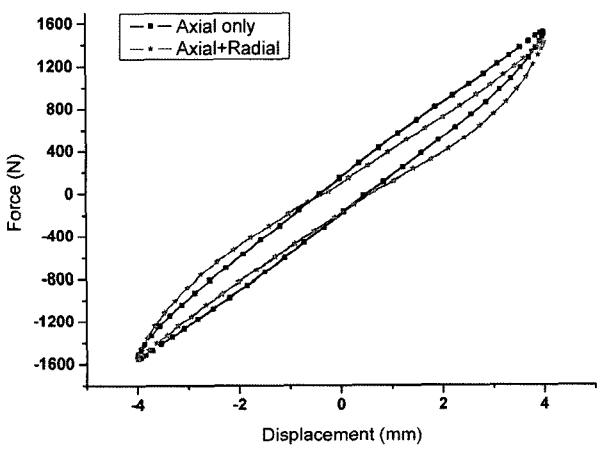

Figure 22. Comparison of bushing forces (axial only versus axial-radial coupled).

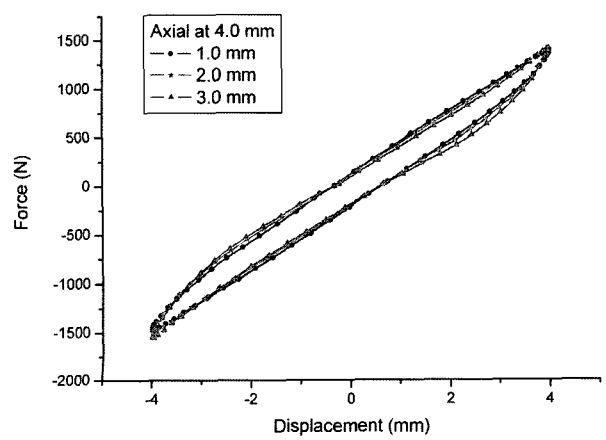

Figure 23. Axial bushing forces according to the different radial input ($\delta_{r,i}$ = 1.0, 2.0, 3.0 mm).

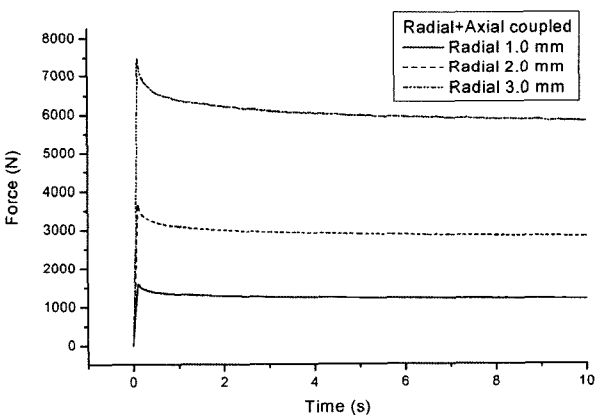

Figure 24. Comparison of radial forces due to 2-axis step input, radial (1.0, 2.0, 3.0 mm) + axial (4.0 mm).

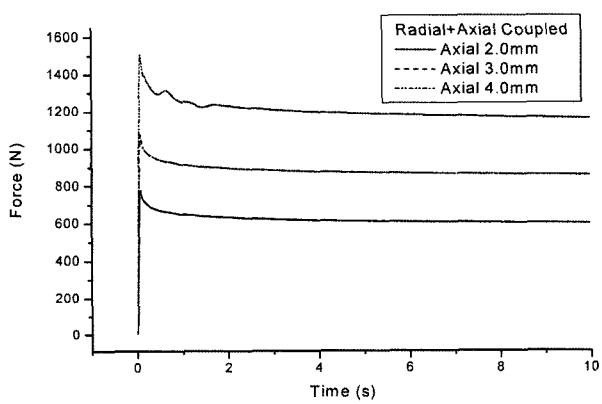

Figure 25. Comparison of axial forces due to 2-axis step input, axial (2.0, 3.0, 4.0 mm) + radial (3.0 mm).

Table 6. Differencies of maximum radial bushing forces due to coupled step input (axial 4.0 mm).

Radial displacement [mm]	Force and error	
	Force [N]	Error [%]
1.0	−16.49	−1.02
2.0	−57.57	−1.56
3.0	−35.27	−0.47

Table 7. Differencies of maximum axial bushing forces due to coupled step input (radial 3.0 mm).

Axial displacement [mm]	Force and error	
	Force [N]	Error [%]
2.0	−202.27	−22.04
3.0	−187.87	−14.89
4.0	−101.01	−6.29

Table 7 presents differencies of the maximum axial bushing forces due to a coupled step input with a 3.0 mm radial input. The maximum force of axial bushing force is about 22% less compared to the result without a radial input. Therefore, the axial bushing force is affected by the radial step input.

3.2. Coupled Test of Radial and Normal

3.2.1. Radial and normal coupled test under sine wave excitation

As shown in the Figure 1, the radial stiffness and the normal stiffness are the same due to symmetry. Radial and normal coupled tests are carried out to analyze how the normal excition affects the radial bushing force. Radial bushing forces with a 3.0 mm radial displacement according to the normal excitations with 1.0, 2.0, and 3.0 mm displacements are shown in the Figure 26. Figure 27

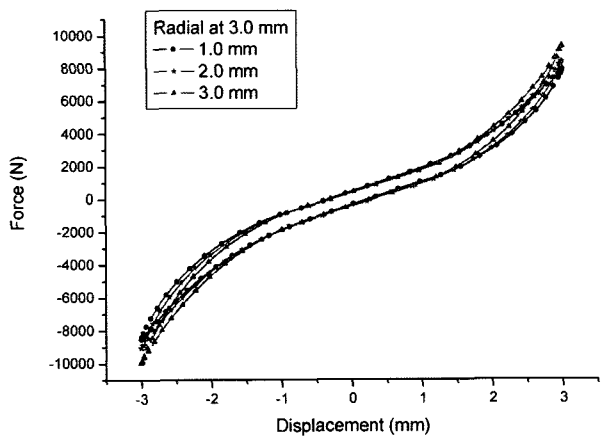

Figure 26. Radial bushing forces according to the normal excitation ($\delta_{r,i}$ = 1.0, 2.0, 3.0 mm).

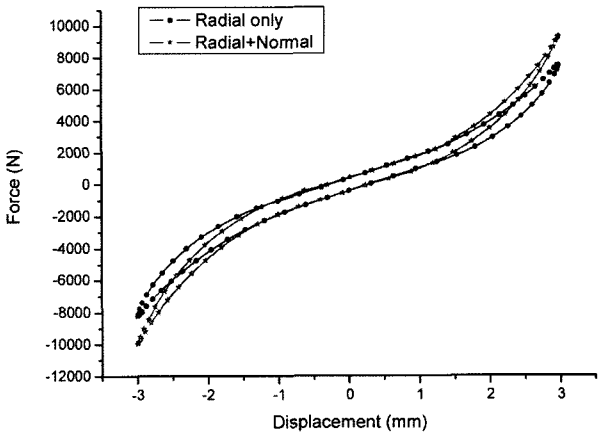

Figure 27. Radial bushing forces with and without normal excitation.

Table 8. Radial slope due to radial-normal coupled excitation (radial 3.0 mm).

Normal displacement [mm]	Slope [N/mm]
0.0	2235.03
1.0	2335.41
2.0	2452.53
3.0	2688.06

presents the comparison of the radial bushing forces between radial only excitation and radial and normal coupled excitation.

According to the test results, normal excitation make the radial bushing forces larger. The slopes according to the excitation displacement are shown in Table 8. When the normal excitation is 3.0 mm, the radial bushing force is 1790 N (about 21.5 %) more than the result without the normal excitation.

3.2.2. Radial and nomal coupled test under step input excitation

Table 9 presents the differencies of maximum forces between the radial step only and radial-normal coupled step input. When the radial step input is 1.0 mm, the difference is small (about 1.47%). However, when the

Table 9. Differencies of the maximum radial bushing forces between the radial only and radial-normal coupled step inputs (normal 3.0 mm).

Radial displacement (mm)	Maximum force	
	(N)	(%)
1.0	−24.15	−1.47
2.0	520.87	13.87
3.0	1607.46	21.34

radial step inputs are over 2.0 mm, the differencies are larger.

3.3. Coupled Test of Radial, Nomal and Axial

3.3.1. Three-axis coupled test under sine wave excitation

Table 10 shows the specifications of the 3-axis coupled tests. The radial bushing forces with 1.0, 2.0, and 3.0 mm sine exciations are analyzed with a 3.0 mm normal and a 4.0 mm axial input. Also, the axial bushing forces with 1.0, 2.0, 3.0, and 4.0 mm sine exciations are analyzed with a 4.0 mm radial and a 3.0 mm normal input.

Figure 28 shows the radial bushing forces with 1.0, 2.0, and 3.0 mm sine excitations under the 3.0 mm normal and 4.0 mm axial sine inputs. Table 11 presents the slopes of the radial bushing forces versus displacement. When the radial inputs are 1.0 and 2.0 mm, the radial bushing forces are smaller than the radial only excitation. However, when the radial input is 3.0 mm, the difference of the slope is about 3% and radial bushing force is mimimally affected by the normal and axial inputs.

Figure 29 shows the radial bushing forces with radial only, radial-axial coupled, and radial-normal-axial coupled sine excitations. Table 12 presents the slopes of the axial bushing forces and relative variations. In table 12, when the radial and axial sine inputs are imposed simultaneously, the slope is decreased by 1.7%. However, when the

Table 10. Specifications of 3-axis coupled tests (radial-axial-normal). (Unit: mm)

Item	Normal	Axial	Radial
Displacements	3.0	4.0	1.0, 2.0 3.0
Item	Radial	Normal	Axial
Displacements	4.0	3.0	1.0, 2.0, 3.0, 4.0

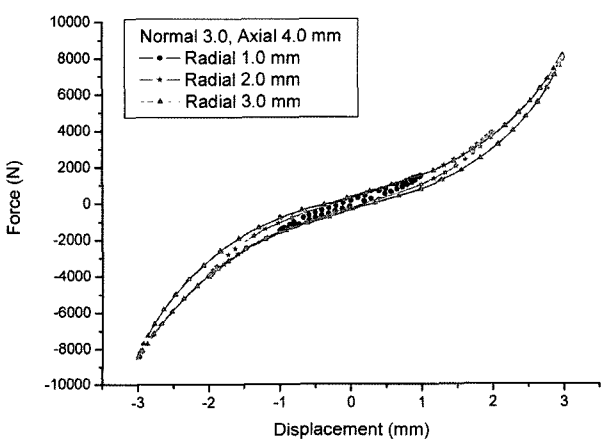

Figure 28. Radial bushing forces (δ_{ri} = 1.0, 2.0, 3.0 mm) under normal 3.0 mm and axial 4.0 mm sine input.

Table 11. Slope comparisons of the radial bushing forces vs displacement between radial only and 3-axis coupled.

Radial displacement [mm]	Slope in 1-axis [N/mm]	Slope in 3-axes [N/mm]
1.0	1811.53	1443.55
2.0	1891.76	1730.17
3.0	2230.03	2300.71

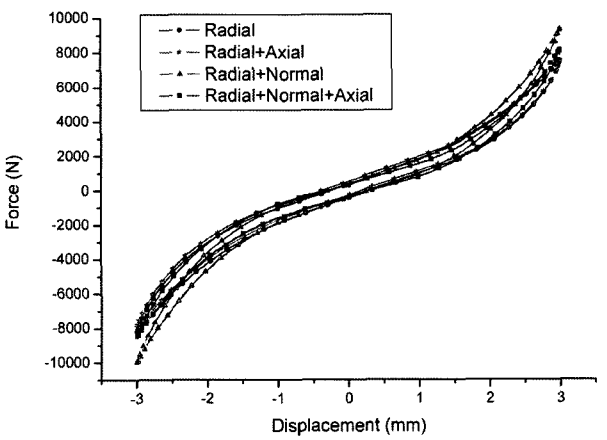

Figure 29. Comparison of radial bushing forces among the radial, radial-axial, radial-normal, and radial-normal-axial coupled.

Table 12. Slope comparisons of the radial bushing forces vs displacement between radial only, radial-axial, radial-normal, and radial-normal-axial coupled.

Axis	Slope [N/mm]	Variation [%]
Radial	2230.03	none
Radial+axial	2191.27	−1.74
Radial+normal	2688.06	20.54
Radial+normal+axial	2300.71	3.17

radial and normal inputs are imposed simultaneously, the slope is increased by 20.5%. When the normal input is imposed, the rubber part of the radial direction is relatively reduced. This makes the stiffness of the radial direction harder. Therefore, the normal input makes the radial bushing force bigger. In addition, the radial-normal-axial coupled test results show a smaller result than the radial-normal coupled result. This is caused by the interaction between the normal and axial directions.

Figure 30 shows the axial bushing forces with 1.0, 2.0, 3.0, and 4.0 mm sine excitations under a 3.0 mm radial and 3.0 mm normal sine inputs. Table 13 presents slopes of axial busihg forces versus the displacement. The axial bushing forces are increasing with respect to the

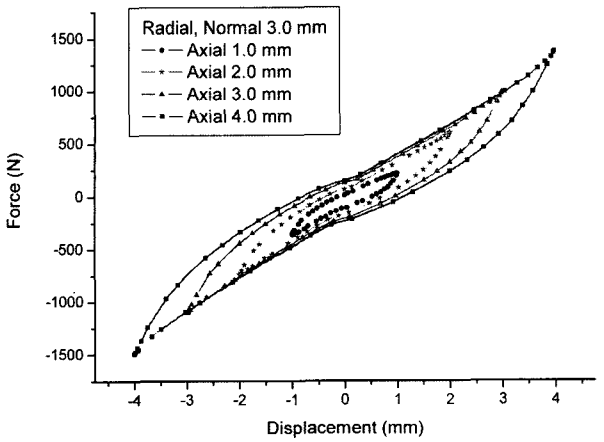

Figure 30. Axial bushing forces ($\delta_{a,i}$ = 1.0, 2.0, 3.0, 4.0 mm) with 3.0 mm radial and 3.0 mm normal inputs.

Table 13. Slopes of axial busihg forces vs displacement.

Axial displacement [mm]	Slope in 1-axis [N/mm]	Slope in 3-axis [N/mm]
1.0	523.37	264.90
2.0	416.10	303.77
3.0	385.98	310.10
4.0	368.84	316.64

displacement. When the axial only input is imposed, the slopes of the bushing force decrease with respect to the displacement. However, when the 3 axes are excited simultaneously, the slopes of the axial bushing force are increased. The radial and normal excitation affect the energy loss of axial direction and increase the pinching phenomenon.

Figure 31 shows the axial bushing forces with an axial only, axial-radial coupled, and axial-radial-normal coupled sine excitations. Table 14 presents the slopes of the axial bushing forces and relative variations. As shown in Figure 31, the maximum axial bushing forces are minimally affected by the radial and normal direction inputs. However, the slopes decrease and the pinching phenomenon increase according to the radial and normal inputs.

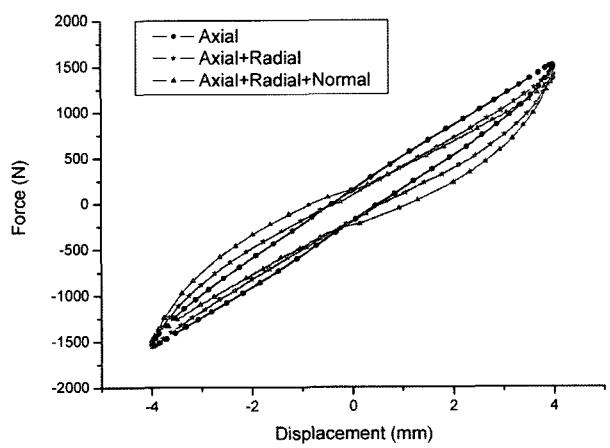

Figure 31. Comparison of axial bushing forces among the axial, axial-radial, and axial-radial-normal coupled.

Table 14. Slope comparisons of the axial bushing forces vs displacement between axial, axial-radial, and axial-radial-normal coupled.

Excitation	Slope [N/mm]	Variation [%]
Axial	368.84	none
Axial+radial	340.93	−7.57
Axial+radial+normal	316.64	−14.15

3.3.2. Three-axis coupled test under step input

Table 15 presents the differencies of maximum radial bushing forces with respect to the radial step inputs under 3.0 mm normal and 4.0 mm axial step inputs during a 0.1 second rise time. As shown in Table 15, when the radial input is 1.0 mm, the radial bushing force is decreased by 7.27%. However, when the radial step inputs are 2.0 and 3.0 mm, the radial bushing forces are increased.

Table 16 presents the differencies of maximum axial bushing forces according to the axial step inputs under 4.0 mm normal and 3.0 mm radial step inputs during a 0.1 s rise time. As shown in Table 16, when the axial input is 2.0 mm, the axial bushing force is decreased by 23.54%. When the axial step input is small, the normal

Table 15. Differencies of maximum radial bushing force due to 3-axis coupled step input (normal 3.0 mm, axial 4.0 mm).

Radial displacement (mm)	Maximum force	
	(N)	(%)
1.0	−117.51	−7.27
2.0	283.40	7.58
3.0	1371.73	18.28

Table 16. Differencies of maximum axial bushing force due to 3-axis coupled step input(radial 3.0 mm, normal 4.0 mm).

Axial displacement [mm]	Force and error	
	Force [N]	Error [%]
2.0	−216.53	−23.54
3.0	−244.79	−19.40
4.0	−91.50	−5.70

and radial step inputs affect the axial bushing force. According to the case of increasing the axial step input, the effects of normal and radial inputs are smaller.

4. CONCLUSIONS

In this study, the rubber bushing characteristics were tested by using a MTS 3-axis rubber tester. Sine wave, step input, and random excitations are imposed on the bushing in the radial and the axial direction. Also, the two-directional coupled tests such as radial-axial radial-normal test were carried out. In addition, 3-axis tests with axial, radial, and normal directions are carried out. From the results obtained through these tests, the following conclusions are obtained.

(1) In the radial only sine excitation tests, the nonlinear characteristics increase when the displacements are higher.

(2) In the axial only sine excitation tests, the axial bushing forces are larger but the slopes of bushing forces versus displacements are lower. There are no nonlinear characteristics.

(3) The results of step inputs show a tendency similar to the sine excitation results within a 5.0% error and bushing forces come reach steady state in 2.8 seconds. Results from the random inputs are similar to the results of sine and step inputs.

(4) From the 2-axis tests, the axial displacements seldom affect the radial bushing forces but the radial displacements make a nonlinear tendency of the axial bushing forces. This is because the bushing used in this study is designed to have mainly radial forces and a radial stiffness about 5 times larger than axial stiffness. The radial and normal stiffness are the same because of geometric symmetry. From the coupled tests, radial bushing forces are increased by 20% due to the deformation in the normal direction.

(5) From the 3-axis tests, in the case of the radial only, radial-axial coupled, and radial-normal-axial coupled tests, the radial bushing forces have similar tendencies to each other. When the 2-axis or 3-axis inputs are imposed on the bushing, radial bushing forces are mainly affected by normal deformation.

(6) Axial bushing forces are sensitive to the normal and radial deformations and the pinching phenomenon is increased due to the radial or normal deformations. However, the maximum axial bushing forces are not changed by the radial or normal inputs.

In this study, the bushing characteristics due to 3-axis excitations are systematically analyzed. When the 1-axis force is applied to the bushing or coupled effects can be neglected, it is not required to make the coupled bushing model. However, the coupled bushing model is necessary to carry out the precise vehicle dynamics analysis in other cases. These test procedures can be available to other tests. Test results can be used to make the accurate bushing model for vehicle dynamic simulations.

ACKNOWLEDGEMENT–This work was supported by the Korea Science and Engineering Foundation (KOSEF) throuth the NRL (National Research Laboratory) Program funded by the Ministry of Science and Technology (NO. M1-0203-00-0017).

REFERENCES

Barber, A. J. (2000). Accurate models for complex vehicle components using empirical methods. *SAE Paper No.* 2000-01-1625.

Choi, B. L., Choi, J. H. and Choi, D. H. (2005). Reliability-based design optimization of an automotive suspension system for enhancing Kinematic and compliance characteristics. *Int. J. Automotive Technology* **6**, **3**, 235–242.

Dzierzek, S. (2000). Experiment-based modeling of cylindrical rubber bushings for the simulation of wheel suspension dynamic behavior. *SAE Paper No.* 2000-01-0095.

FunctionBay, Inc. (2005). *RecurDyn Theoretical Manual Ver. 6.1*. Korea.

Kuo, E. Y. (1997). Testing and characterization of elastomeric bushing for large deflection behavior. *SAE Paper No.* 970099.

Lee, S. B. and Wineman, A. (2000). A model for nonlinear viscoelastic coupled mode response of an elastomeric bushing. *Int. J. Non-Linear Mech.*, **35**, 177–199.

MSC Software Corporation (2003). *ADAMS User's Manual*. USA.

Ok, J. K., Park, D. W., Yoo, W. S. and Sohn, J. H. (2006). Development of a new bushing model for vehicle suspension module design. *Trans. Korean Society of Automotive Engineers* **14**, **6**, 143–150.

SAE Recommended Practice (1994). Elastomeric bushing "TRAC" application code. *SAE J.* **1883**.

Sohn, J. H., Lee, S. K., Ok, J. K. and Yoo, W. S. (2007). Comparison of semi-physical and black-box bushing model for vehicle dynamics simulation. *J. Mechanical Science and Technology* **21**, **2**, 264–271.